



ORIGINAL ARTICLE

# Shear in sand-lightweight and conventional high strength concrete through the push-off test

*Cisalhamento em concreto leve e convencional de alta resistência através do ensaio push-off*

Patricia da Silva Pereira Figueiredo<sup>a</sup> Thais Amaral Soares<sup>a</sup> Sergio Luis González García<sup>a</sup> Allonso Curty da Silva Pereira<sup>a</sup> Juliana Corrêa Trindade<sup>a</sup> <sup>a</sup>Universidade Estadual do Norte Fluminense Darcy Ribeiro – UENF, Laboratório de Engenharia Civil, Campos dos Goytacazes, RJ, BrasilReceived 20 August 2018  
Accepted 10 August 2020

**Abstract:** Shear design models in reinforced concrete structures depend on stress transfer through cracks. Such mechanism is influenced by the displacement and roughness of the opposite faces generated during cracking. Shear is reduced when an aggregate particle is fractured leading to a smoother crack as found in lightweight and high strength concrete. This study evaluated the ultimate shear strength of sand-lightweight and conventional high strength concrete as well as the differences in their behavior. Results from Pereira and Soares with 29 push-off test specimens were used. Transverse clamping stress ranged from 4.79 to 12.71 MPa while  $f_{cm}$  was 30 and 50 MPa. The experimental results showed significant differences in the concrete studied. A tri-linear model was proposed to calculate the ultimate shear strength. An overall mean value of  $\tau_{u, exp}/\tau_{u, cal}$  was 0.96.

**Keywords:** shear-friction, lightweight concrete, high-strength concrete.

**Resumo:** Os modelos de dimensionamento ao cisalhamento em estruturas de concreto armado dependem da transferência de esforços através das fissuras, tal mecanismo é influenciado pelo deslocamento e rugosidade das faces opostas geradas durante a fissuração. O cisalhamento é reduzido quando a partícula do agregado se fratura, levando à fissura mais lisa, como ocorre em concretos leve e de alta resistência. O trabalho objetiva avaliar a resistência última de cisalhamento de concretos leve e convencional de alta resistência, mostrando-se as diferenças no comportamento dos mesmos. Para tal, foram utilizados os resultados de Pereira e Soares, com 29 corpos de prova *push-off*, com tensão de confinamento variando de 4,79 a 12,71 MPa e  $f_{cm}$  de 30 e 50 MPa. Os resultados experimentais exibiram diferenças significativas nos concretos estudados. Foi proposto um modelo trilinear para calcular resistência última de cisalhamento, com valor de média geral da relação  $\tau_{u, exp}/\tau_{u, cal}$  de 0,96.

**Palavras-chave:** atrito-cisalhamento, concreto leve, concreto alta resistência.

**How to cite:** P. S. P. Figueiredo, T. A. Soares, S. L. González García, A. C. S. Pereira, and J. C. Trindade, "Shear in sand-lightweight and conventional high strength concrete through the push-off test," *Rev. IBRACON Estrut. Mater.*, vol. 14, no. 3, e14307, 2021, <https://doi.org/10.1590/S1983-41952021000300007>

## 1 INTRODUCTION

Proposed by Birkeland and Birkeland [1] in 1966, the shear-friction theory is an approach that aims to evaluate the transfer of shear forces in concrete-concrete interfaces submitted at the same time by compression and shear stresses. According to the shear-friction theory, these stresses are strengthened exclusively by friction.

Corresponding author: Sergio Luis González García. E-mail: liluiser@yahoo.com.br

Financial support: The study was funded in part by the Coordenação de Aperfeiçoamento de Pessoal de Ensino Superior (CAPES) - Funding Code 001.

Conflict of interest: Nothing to declare.



This is an Open Access article distributed under the terms of the Creative Commons Attribution License, which permits unrestricted use, distribution, and reproduction in any medium, provided the original work is properly cited.

According to Hsu et al. [2], the shear transfer mechanism occurs in two different ways: shear transfer through an initially uncracked plane or shear transfer through an initially cracked plane.

In the first shear transfer mechanism, inclined cracks occur to the shear plane, which results in strut and tie-type action. In the second one, initial cracks prevent the development of the truss action. Under shear stress, the concrete element on one side of the crack slides to the other. The sliding is accompanied by an increase in cracks due to the roughness and irregularities along the surface.

This served as a basis for the application of the shear-friction theory that assesses the capacity of a crack to transfer shear forces in structural concrete.

According to González Fonteboa et al. [3], the factors that influence the friction-shear capacity are aggregate interlock, friction, compression force applied perpendicular to interface, the reinforcement across the shear plane and concrete strength.

A model denominated a saw-tooth is commonly used to exemplify the mechanisms involved in this theory. According to Santos and Júlio [4], the model considers the influence of the reinforcement placed crossing the interface and the external forces acting perpendicularly to the shear plane.

In the model, the rough interface is replaced by a series of small teeth. When a horizontal force is applied, one part will slide over the other. Due to the presence of the teeth, the sliding is accompanied by a separation of the surface and this pulls the transverse reinforcement through the interface. To keep a balance, the reinforcement generates compression stresses at the interface and the sliding generates bending and shear forces. Thus, the shear is transmitted due to the aggregates interlock on the cracked surface, friction, and the reinforced shear strengths by dowel action.

The friction and the aggregate interlock are results of the cracked face roughness and are increased by the normal compression force at the interface. The contribution of concrete strength is related to the rupture of the interface, which transmits shear forces and results in loss of contact due to the crushing of the aggregates and the cement matrix. The crushing occurs when the constituents reach their capacity, which is related to the concrete strength.

Concrete can be represented as a system consisting of two phases: the matrix and the particles incorporated into it. The contact area between the two materials is called the interface zone. Generally, the parameters of strength and rigidity of the matrix are lower than those of the particle aggregate. However, the interface zone is the weakest link in this system. Thus, the cracks normally propagate through the matrix, around the aggregates [5].

Considering the shear plane of lightweight concrete, the slip strength is lower than the one in conventional concrete. This occurs because the lightweight aggregate allows the cracks to cross the aggregate instead of moving around it, as in conventional concrete. In other words, cracking is linked to the rupture of aggregate since the strength is comparable to the matrix strength and the “face-smooth crack” results in a less efficient transfer of shear-friction through the aggregate interlock [6].

The High-strength concrete matrix has a higher compressive strength compared to conventional concrete. Thus, the behavior presented by high-strength concrete is similar to lightweight concrete with regard to rupture mode where cracks cross the aggregate.

Few experimental studies have been performed to determine the shear-friction characteristics in concrete with lightweight aggregates [7]–[9]. Some studied the various origins of aggregates [10] and others tried to develop high-efficiency concrete [11], [12].

Push-off test models were used to develop this study. The model has been often used because it requires small-sized specimens, it is cheap and easy to perform and highly specialized test equipment is not needed. The specimens are formed by two L-shaped parts, with two openings that delimit them which allow sliding between them. It has a section reduction in the direction of the shear plane (Figure 1). It also has an auxiliary reinforcement to not allow premature rupture by bending stresses in external phases.

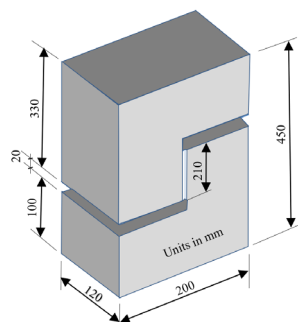


Figure 1. Push-off specimen dimensions.

## 2 JUSTIFICATION

According to Santos and Júlio [13], the friction-shear theory was adopted in most design codes to analyze the concrete-concrete interfaces, and over the past years, it has received several suggestions for improvements to increase accuracy and field application.

Even though it has received many contributions, the ultimate shear capacity has not been fully designed yet for being a complex phenomenon. Currently proposed models and standards to determine ultimate shear capacity present significant differences with respect to experimental values.

We aim to contribute to the development of shear-friction theory and its application in sand-lightweight concrete and conventional high-strength concrete. The main variables studied were clamping stress ( $\rho_v f_{yd}$ ), concrete compressive strength ( $f_{cm}$ ), and coarse aggregate type (lightweight expanded clay aggregate and conventional granite gravel aggregate). We compared the experimental results obtained in these studies with analytical models and prescriptions of ACI 318 [14] and proposed a tri-linear model for the determination of the ultimate shear capacity with greater reliability.

## 3 MATERIALS AND EXPERIMENTAL PROGRAM

This paper analyzed results obtained by Pereira [15] and Soares [16]. Both studies used Mizu<sup>®</sup> high-initial-strength Portland cement (CP V). Quartz sand from Paraíba do Sul River (Campos dos Goytacazes, Brazil) was used as a fine aggregate. Two types of coarse aggregates were used: CINEXPAN<sup>®</sup> expanded spherical clay type 1506 with an average diameter of 12.5 mm, and granite type gravel from crushing stones from Campos dos Goytacazes region.

The maximum diameter, the fineness module and the real specific mass of the aggregates were calculated according to ABNT NBR NM 248 [17] and ABNT NBR-NM 45 [18]. The results for granite gravel were 19.00 mm, 5.65 mm and 2.90 kg/dm<sup>3</sup> respectively. The values for expanded clay were 12.5 mm, 3.6 mm and 1.15 kg/dm<sup>3</sup>. Viapol<sup>®</sup> PLASTOL 5035 was used as the superplasticizer and the water used was supplied by Águas do Paraíba, the company responsible for water supply.

GERDAU CA-50 ribbed bars were used as transverse reinforcement and auxiliary reinforcements. They had nominal diameters of 8 mm and 12.5 mm. For the 8-mm transverse reinforcement, it was obtained a yield strength ( $f_y$ ) of 570 MPa and yield deformation of 2.3%.

Table 1 shows the four concrete compositions produced: one for sand-lightweight concrete and three for high-strength conventional concrete, having  $f_{cm}$  of approximately 30 and 50 MPa, respectively. The slump test value for all compositions was 70 ± 10 mm.

**Table 1.** Composition of concrete used in research (kg/m<sup>3</sup>).

Type of Concrete	Water	Materials					
		Cement	Sand	Gravel	Expanded Clay	W/C	SP (%)
Sand-Lightweight (series A and D)	196.5	517	672.1	-	361.9	0.38	-
Conventional 1 (series B)	205	456	682	1005	-	0.45	-
Conventional 2 (series C)	164.4	478	905.3	860	-	0.34	0.83
Conventional 3 (series E)	225.8	511.6	719.77	905.2	-	0.44	1.47

SP - superplasticizer; W/C - water/cement ratio.

To achieve the proposed objectives, 29 initially cracked push-off specimens from Pereira [15] and Soares [16] were manufactured and tested, under constant monotonous load. The experimental program was divided into five series: A, B and C produced by Pereira [15], and D and E, produced by Soares [16]. The nomenclature adopted for the specimens was: Xn-PO-Y-Z, where X specifies the type of concrete, n specifies the number of concrete (when there is more than one), PO refers to the push-off test, Y is the type of composition and Z was the clamping stress of the transverse reinforcement.

The dimensions of push-off specimens were defined considering ranges used by previous studies, as shown in Pereira [15]. Transverse reinforcements were those commonly used in concrete submitted to this type of stress. The auxiliary reinforcement was defined through stress analysis using SAP 2000<sup>®</sup> software, allowing the flow of compressive stresses (strut) and tensile stresses (tie) to be found and subsequently sized using the model of connecting strut and tie, by CAST<sup>®</sup> software, both shown in Figure 2. Details of the push-off specimens are shown in Figure 3.

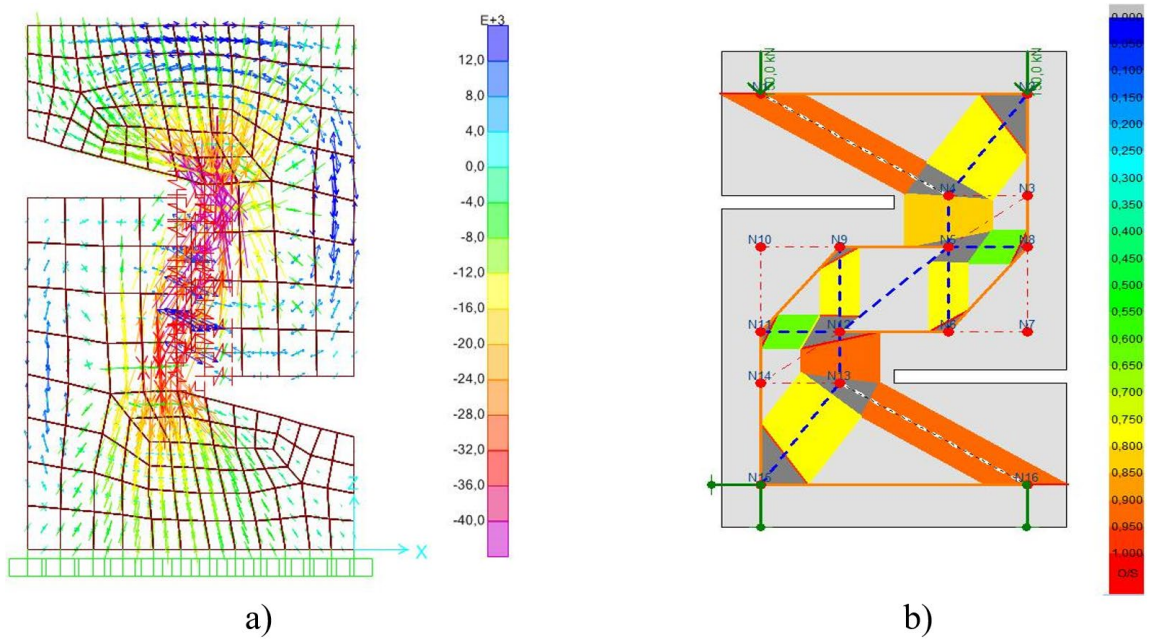


Figure 2. Push-off specimen stress analysis: a) main stress distribution using SAP software (2000)<sup>®</sup> and b) strut and tie model using the software CAST<sup>®</sup> [15].

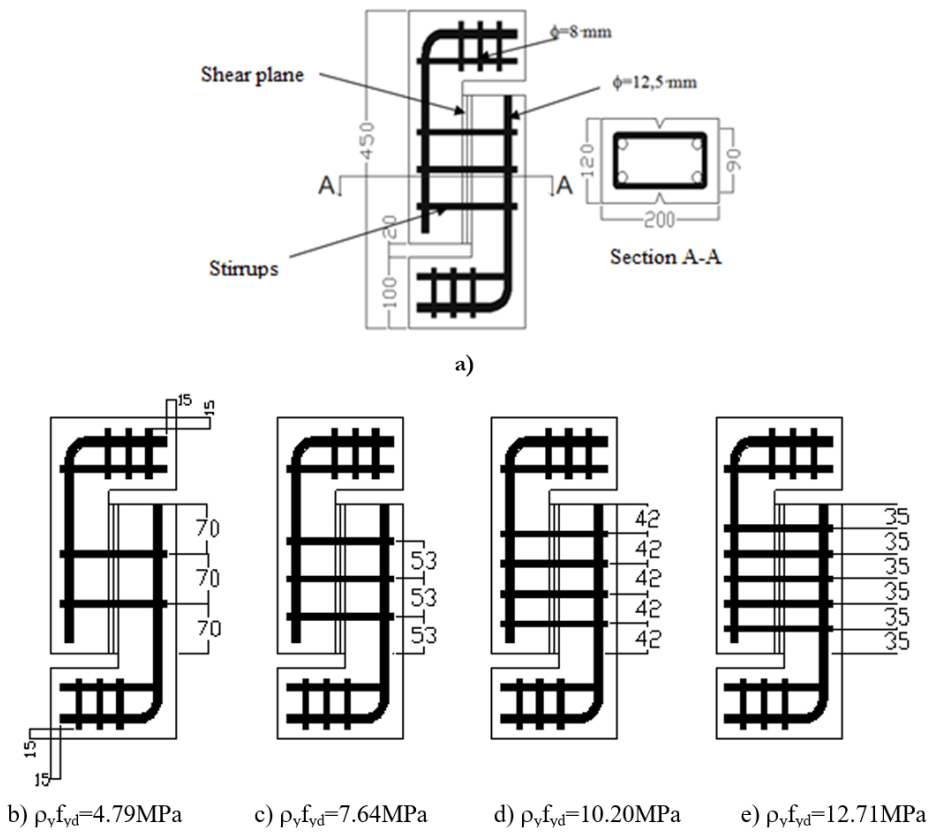


Figure 3. Transverse and auxiliary reinforcements on push-off specimens: a) specimen dimensions (mm); b), c) e d) series A, B, C, D and E and e) series A, B e C.

To manufacture push-off specimens, metal forms were made as shown in Figure 4. They had a protrusion at the bottom and at the top to delimit the shear plane. Two Styrofoam plates fixed to the form were used for the opening at the ends.

The compressive strength of the concrete was evaluated by rupture cylindrical specimens with dimensions of 100 mm in diameter and 200 mm in height, according to ABNT NBR 5739 [19]. The splitting tensile strength was determined using cylindrical specimens with the same geometrical characteristics and in accordance with the ABNT NBR 7222 [20]. Both results are shown in Table 2.



Figure 4. Metallic form for the production of push-off specimens [15].

The push-off specimens were initially cracked. For this purpose, steel rollers were placed in the shear plane of the specimen in the horizontal position, applying a constant linear load. The tests were performed on an EMIC® test machine with capacity of 2000 kN until the initial point of pre-cracking was detected. The diagram and the pre-cracking test are shown in Figure 5.

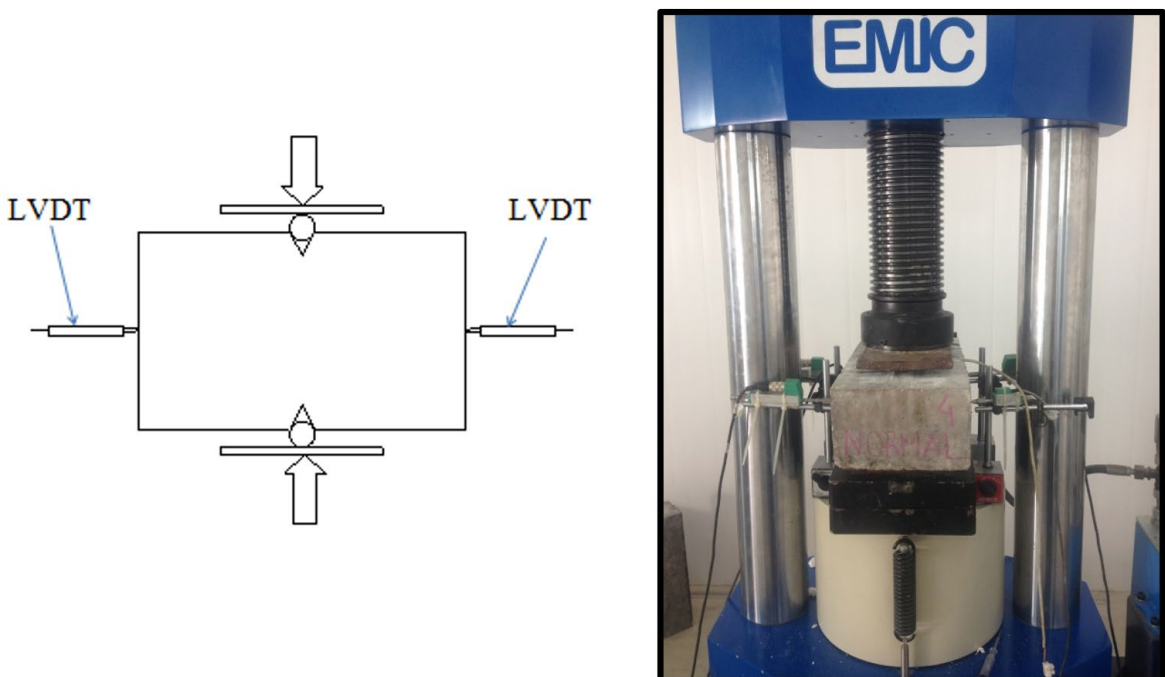


Figure 5. Instrumentation schematic of the push-off pre-cracking test specimens [15].

**Table 2.** Results of compression, splitting tensile and direct shear tests.

Series	Specimens	$f_{cm}$ (MPa)	$f_{ct, sp}$ (MPa)	$\tau_{u, exp}$ (MPa)	$\tau_{u, exp}/f_{cm}$	$\rho_v f_{yd}/f_{cm}$
A	L-PO-1- 4.79	30.9	1.9	4.2	0.14	0.16
	L-PO-1- 7.64			4.3	0.14	0.25
	L-PO-1-10.20			5.6	0.18	0.33
	L-PO-1-12.71			5.7	0.18	0.41
B	N-PO-1- 4.79	52.2	3.2	5.8	0.11	0.09
	N-PO-1- 7.64			8.5	0.16	0.15
	N-PO-1-10.20			10.1	0.19	0.20
	N-PO-1-12.71			7.5	0.14	0.24
C	N-PO-2- 4.79	50.3	3.0	6.4	0.13	0.10
	N-PO-2- 7.64			7.5	0.15	0.15
	N-PO-2-10.20			7.8	0.16	0.20
	N-PO-2-12.71			8.9	0.18	0.25
D	L1-PO-1- 4.79	26.2	2.5	3.9	0.15	0.18
	L2-PO-1- 4.79			5.9	0.22	0.18
	L3-PO-1- 4.79			3.4	0.14	0.19
	L1-PO-1- 7.64			5.1	0.19	0.29
	L2-PO-1- 7.64			5.3	0.19	0.28
	L3-PO-1- 7.64			7.2	0.29	0.30
	L1-PO-1-10.20			4.9	0.19	0.39
	L2-PO-1-10.20			5.5	0.20	0.38
	L3-PO-1-10.20			4.5	0.18	0.41
E	N1-PO-3- 4.79	54.0	4.3	5.2	0.09	0.08
	N2-PO-3- 4.79			5.9	0.12	0.10
	N3-PO-3- 4.79			5.5	0.10	0.09
	N1-PO-3- 7.64			6.6	0.11	0.13
	N2-PO-3- 7.64			5.7	0.11	0.15
	N3-PO-3- 7.64			7.2	0.13	0.14
	N2-PO-3-10.20			6.9	0.14	0.20
	N3-PO-3-10.20			7.2	0.13	0.19

where:  $f_{cm}$  is the compressive strength of concrete.  $f_{ct, sp}$  is the splitting tensile strength,  $\tau_u$  is the ultimate shear strength and  $\rho_v f_{yd}$  is the clamping stress of the transverse reinforcement.

After pre-cracking preparation, the specimens were instrumented by four GEFTRAN® brand variable linear displacement transducers (LVDTs) with a 5 mm stroke and 0.98 calibration constants. Subsequently, they were submitted to direct shear testing as shown in Figure 6.



**Figure 6.** Set of steel plates and rollers for the direct shear test of push-off specimens [15].

Two LVDTs were positioned vertically to measure the slip of one part of the specimen relative to the other and the other two were positioned horizontally to measure the horizontal displacement. The results were recorded by Lynx Technology's AqDados® 7.5.

The push-off specimens were tested using an EMIC® universal testing machine with a capacity of 2000 kN by placing a spherical seat and a set of steel plates and rollers to ensure that the separation of the two halves of the specimen was not restricted by the testing machine as shown in Figure 7. The load application speed was 0.3 mm/s.

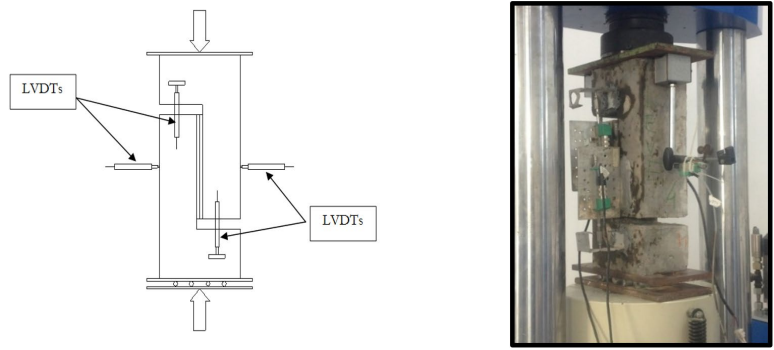


Figure 7. Instrumentation schematic and direct shear testing of push-off specimens [15].

## 4 RESULTS AND DISCUSSIONS

### 4.1 The behavior of push-off specimens

Figure 8a shows the rupture mode of push-off specimens that cracked by shear in the initial cracked plane. L-PO-1-12.71 and N-PO-1-12.71 which ruptured by the combination of bending and shear, as shown in Figure 8b. The flexion occurred on the outer faces as previously reported by Kahn and Mitchell [21], and Shaw and Sneed [22].

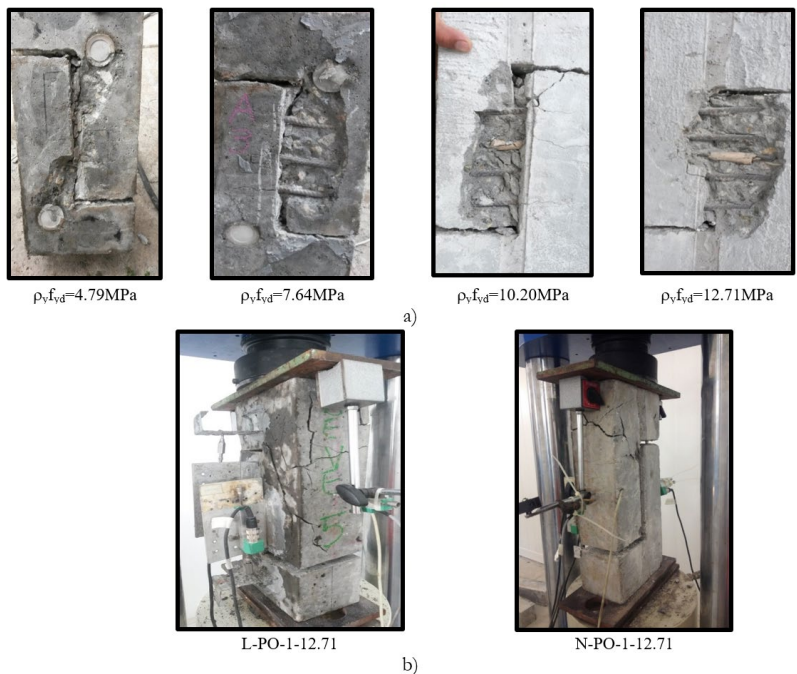


Figure 8. Modes of shear failure of push-off specimens: a) shear plane failure, b) bending and shear combination failure [15].

Figure 9 shows the shear stress variation normalized by  $f_{cm}$  versus slip for sand-lightweight concrete (series A and D) and high-strength conventional concrete (series B, C, and E), respectively, produced by Pereira [15] and Soares [16].

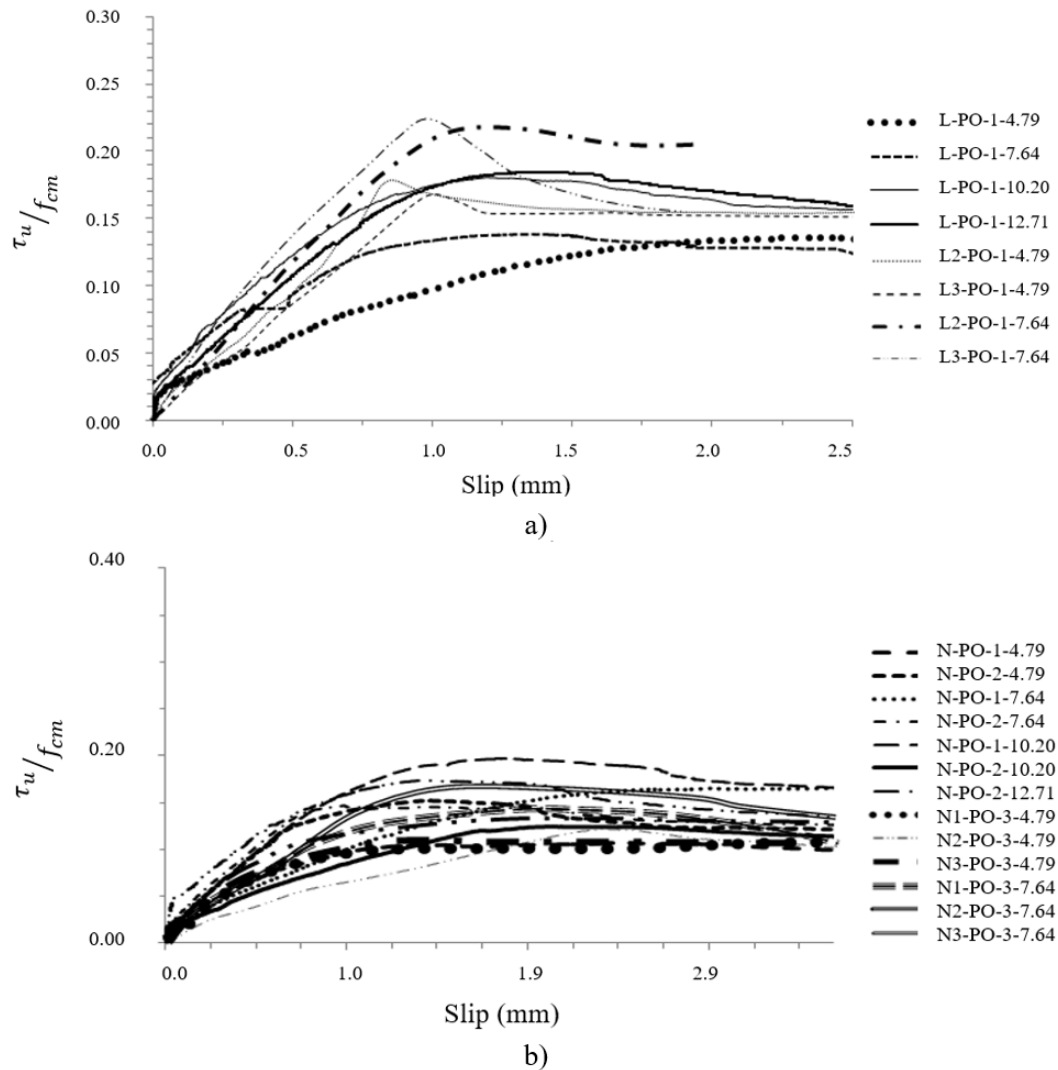
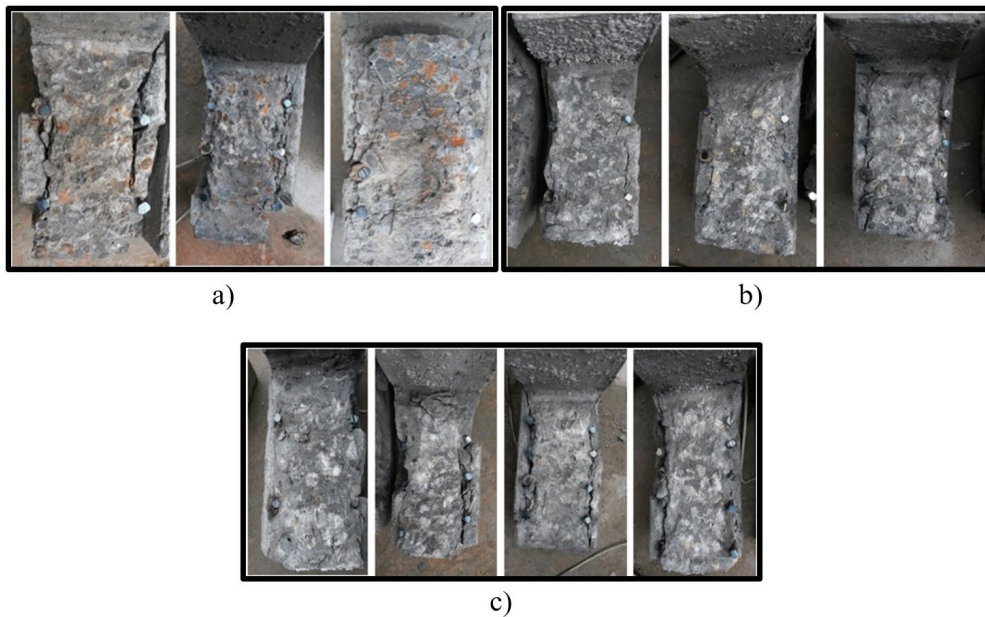


Figure 9. Normalized shear stress vs. slip curves: a) sand-lightweight concrete; b) conventional high-strength concrete.

Similar behavior was noticed for both concrete groups which was an increase in the ultimate shear capacity ( $\tau_u$ ) with an increase in the shear stress ( $\rho_v f_{yd}$ ). The initial stiffness is characterized by the steep rising of the curve at the beginning, which tends to decrease with an increase in load application after reaching the maximum shear strength. Then, there is a gradual reduction in strength and a rise in longitudinal displacement. This behavior is expected for initially cracked push-off specimens as reported by Mansur et al. [23] and Emiko et al. [6].

After performing the push-off tests, the specimens were divided into two parts for a further analysis of the shear place surface. It was found the increase in degree of clamping stress provided by the transverse reinforcement resulted in a smoother surface. For sand-lightweight concrete and conventional high-strength concrete (Figures 10a and 10b), the surface was smoother regardless of the transverse reinforcement rate. For sand-lightweight concrete, there was no rupture of the expanded clay by grinding or shear. However, the rupture was caused by traction rupture. “White points” appeared in the matrix surrounding the expanded clay. For conventional high-strength concrete, there was a growth in these white points (regions?), especially in large aggregate. This was caused by increased interlock between the aggregates in the shear plane. For conventional low-strength concrete, the surface has become rougher (Figure 10c).



**Figure 10.** Rupture surfaces: a) sand-lightweight concrete, b) high-strength concrete and c) low-strength concrete.

#### 4.2 Ultimate shear strength

Table 2 shows the results of the compression tests, splitting tensile strength and last normalized strength. Figure 11 shows the values obtained for the last normalized strength ( $\tau_u/f_{cm}$ ) versus normalized clamping stress by concrete strength ( $\rho_v f_{yd}/f_{cm}$ ) to assess the influence of the clamping stress on the ultimate shear capacity between series. The individual values of each push-off specimen for the series A and D (sand-lightweight concrete) and series B, C, and E (high-strength conventional concrete) are presented in Table 2. It was noticed that concrete produced with expanded clay has lower shear strength when compared to concrete produced with conventional aggregate. Gerritse [24], Mattock et al. [8] and Emiko et al. [6] have previously reported and confirmed cracks go through the light aggregate, differently from what is observed in conventional concrete aggregate where cracks move around the aggregate. It can be inferred that cracking is linked to the aggregate rupture.

It is observed that, in general, an increase in clamping stress leads to an increase in ultimate shear strength.

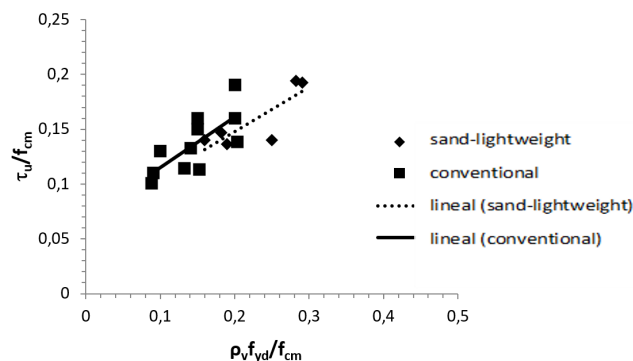
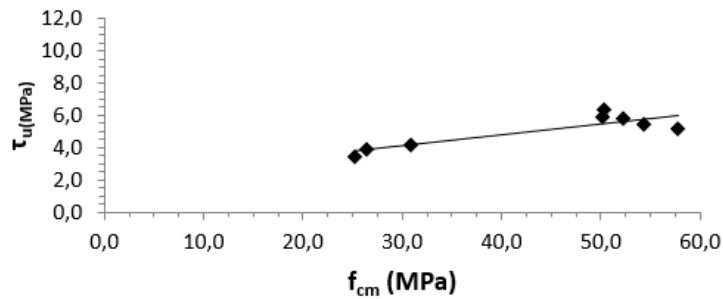


**Figure 11.** Influence of the clamping stress of the transverse reinforcement ( $\rho_v f_{yd} / f_{cm}$ ) in ultimate shear capacity.

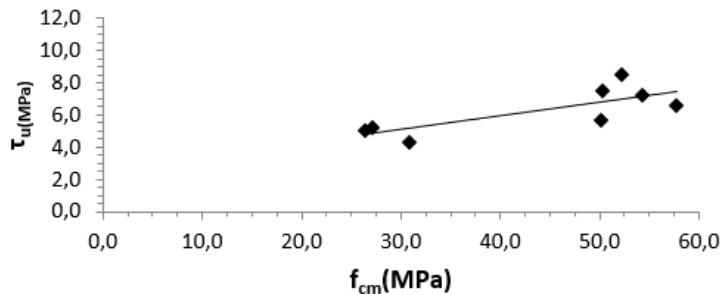
#### 4.3 Influence of concrete compressive strength on ultimate shear capacity

Figure 12 shows the individual values of ultimate shear strength ( $\tau_{u,exp}$ ) versus concrete compressive strength ( $f_{cm}$ ), for all series and the different clamping stress ( $\rho_v f_{yd}$ ) studied. It is observed that the ultimate shear strength becomes greater as concrete compressive strength increases. This is mainly because of aggregate interlock, which the more

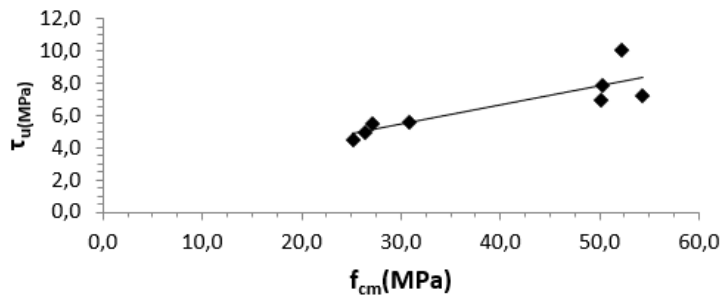
effective it is, the higher the concrete strength value. In concrete with sand-lightweight aggregate, cracks penetrate more easily through the aggregate instead of occurring around the aggregate, as in concrete with normal weight and low strength. The slope (m) of each curve was greater with an increase of ( $\rho_v f_{yd}$ ). The values were 0.0697, 0.0834, 0.1189, at clamping stresses of 4.79, 7.64, 10.20, respectively. It is noticed that for the clamping stress of 12.71 MPa, the slope was 0.1170, being lower when compared with the clamping stress of 10.20 MPa. This was probably due to the few data evaluated, and also, to the ruptured specimens influenced by bending.



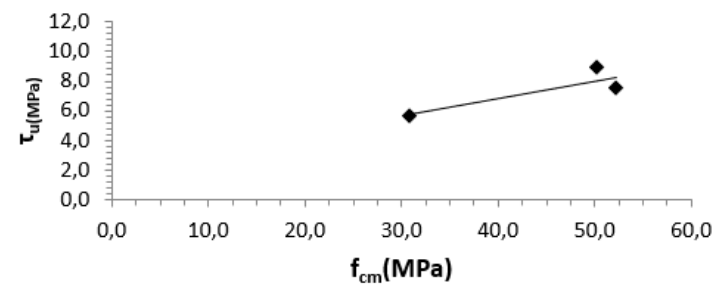
a)  $\rho_v f_{yd} = 4.79$  MPa



b)  $\rho_v f_{yd} = 7.64$  MPa



c)  $\rho_v f_{yd} = 10.20$  MPa



d)  $\rho_v f_{yd} = 12.71$  MPa

**Figure 12.** Influence of concrete compressive strength on the ultimate shear capacity for different clamping stresses.

#### 4.4 Comparison of the ultimate shear strength obtained experimentally with proposed models

Table 3 shows the experimental ultimate shear strength values ( $\tau_{u,exp}$ ) and the calculated values ( $\tau_{u,cal}$ ) obtained by the models proposed by Mattock et al. [8], [25], [6], [26], [23].

Table 4 shows the relationship between the ultimate shear strength ( $\tau_{u,exp}$ ) and the calculated ultimate shear strength ( $\tau_{u,cal}$ ) as prescribed by ACI 318 [14].

The average value and standard deviation of ( $\tau_{u,exp}/\tau_{u,cal}$ ) of series A, B, C, D, and E were 1.20 and 0.35; 1.65 and 0.45; 1.58 and 0.45; 1.42 and 0.47; and 1.54 and 0.37, respectively.

It was noticed that series A having clamping stress of 4.79 MPa showed experimental strength 70% higher than the one calculated by ACI 318 [14]. For clamping stress of 7.64 MPa and 10.20 MPa, the increase was 10%.

In series B, for clamping stress of 4.79 MPa, the experimental strength was 100% higher than calculated ACI 318 [14]. For specimens having clamping stress of 7.64 MPa and 10.20 MPa, this ratio was 90% and 70% higher, respectively.

In series C, the experimental strength was 120% higher for samples having clamping stress of 4.79 MPa compared to those calculated by ACI 318 [14]. For clamping stress of 7.64 MPa, 10.20 MPa, and 12.71 MPa, this ratio was 60%, 30%, and 20% higher, respectively.

**Table 3.** Ultimate shear strength values obtained experimentally and the calculated values of proposed models.

Series	Specimens	$\tau_{u,exp}$ (MPa)			$\tau_{u,calc}$ (MPa)			
		[15], [16]	[8]	[25]	[6]	[26]	[23]	
A	L-PO-1- 4.79	4.20	5.53	5.78	5.35	-	-	
	L-PO-1- 7.64	4.27	7.81	7.31	6.76	-	-	
	L-PO-1-10.20	5.56	9.86	8.44	7.81	-	-	
	L-PO-1-12.71	5.70	11.87	9.42	8.72	-	-	
B	N-PO-1- 4.79	5.84	-	-	-	9.05	8.95	
	N-PO-1- 7.64	8.50	-	-	-	11.33	11.3	
	N-PO-1-10.20	10.13	-	-	-	13.38	13.06	
	N-PO-1-12.71	7.54	-	-	-	15.39	14.58	
C	N-PO-2- 4.79	6.38	-	-	-	8.86	8.78	
	N-PO-2- 7.64	7.52	-	-	-	11.14	11.09	
	N-PO-2-10.20	7.8	-	-	-	13.19	12.82	
	N-PO-2-12.71	8.89	-	-	-	15.2	14.31	
D	L1-PO-1- 4.79	3.86	5.53	5.79	4.71	-	-	
	L2-PO-1- 4.79	5.90	5.53	5.79	4.77	-	-	
	L3-PO-1- 4.79	3.44	5.53	5.79	4.61	-	-	
	L1-PO-1- 7.64	5.06	7.81	7.31	5.65	-	-	
	L2-PO-1- 7.64	5.25	7.81	7.31	5.71	-	-	
	L3-PO-1- 7.64	7.20	7.81	7.31	5.55	-	-	
	L1-PO-1-10.20	4.91	9.86	8.44	6.49	-	-	
	L2-PO-1-10.20	5.51	9.86	8.44	6.56	-	-	
	L3-PO-1-10.20	4.51	9.86	8.44	6.40	-	-	
E	N1-PO-3- 4.79	5.21	-	-	-	8.45	8.55	
	N2-PO-3- 4.79	5.89	-	-	-	7.84	8.06	
	N3-PO-3- 4.79	5.48	-	-	-	8.18	8.33	
	N1-PO-3- 7.64	6.58	-	-	-	10.73	10.12	
	N2-PO-3- 7.64	5.68	-	-	-	10.12	9.62	
	N3-PO-3- 7.64	7.20	-	-	-	10.46	9.90	
	N2-PO-3-10.20	6.92	-	-	-	12.17	11.03	
	N3-PO-3-10.20	7.23	-	-	-	12.51	11.31	

**Table 4.** Relationship between ultimate shear strength ( $\tau_{u, exp}$ ) and calculated ultimate shear strength ( $\tau_{u, cal}$ ) according to the requirements of the ACI 318 [14].

Series	Specimens	$\tau_{u, cal}$ [14]	$\tau_{u, exp}$	$\tau_{u, exp}/\tau_{u, cal}$	Average	SD
A	L-PO-1-4.79	2.4	4.2	1.7	1.20	0.35
	L-PO-1-7.64	3.9	4.3	1.1		
	L-PO-1-10.20	5.2	5.6	1.1		
	L-PO-1-12.71	6.5	5.7	0.9		
B	N-PO-1-4.79	2.9	5.8	2.0	1.65	0.45
	N-PO-1-7.64	4.6	8.5	1.9		
	N-PO-1-10.20	6.1	10.1	1.7		
	N-PO-1-12.71	7.6	7.5	1.0		
C	N-PO-2-4.79	2.9	6.4	2.2	1.58	0.45
	N-PO-2-7.64	4.6	7.5	1.6		
	N-PO-2-10.20	6.1	7.8	1.3		
	N-PO-2-12.71	7.6	8.9	1.2		
D	L1-PO-1-4.79	2.4	3.9	1.6	1.42	0.47
	L2-PO-1-4.79	2.4	5.9	2.4		
	L3-PO-1-4.79	2.4	3.4	1.4		
	L1-PO-1-7.64	3.9	5.1	1.3		
	L2-PO-1-7.64	3.9	5.3	1.4		
	L3-PO-1-7.64	3.9	7.2	1.8		
	L1-PO-1-10.20	5.2	4.9	0.9		
	L2-PO-1-10.20	5.2	5.5	1.1		
	L3-PO-1-10.20	5.2	4.5	0.9		
E	N1-PO-1-4.79	2.9	5.2	1.8	1.54	0.37
	N2-PO-1-4.79	2.9	5.9	2.1		
	N3-PO-1-4.79	2.9	5.5	1.9		
	N1-PO-1-7.64	4.6	6.6	1.4		
	N2-PO-1-7.64	4.6	5.7	1.2		
	N3-PO-1-7.64	4.6	7.2	1.6		
	N2-PO-1-10.20	6.1	6.9	1.1		
	N3-PO-1-10.20	6.1	7.2	1.2		

SD- Standard Deviation

It was observed that the average experimental strength for clamping stress of 4.79 MPa was 80% higher than calculated by ACI 318 [14] for series D. For clamping stress of 7.64 MPa in this series, the percentage was 50% higher than calculated.

For series E, the average experimental strength for clamping stress of 4.79 MPa was 93% higher than calculated by ACI 318 [14]. For 7.64 MPa clamping stress, the percentage was 40% higher.

For specimens having 12.71 MPa of clamping stress from series A and B and the ones having 10.20 MPa of clamping stress from series D and E, the values were lower than those calculated taking into account ACI 318 [14] requirements. This was caused by the influence of bending rupture, which occurred by over-covering, limiting the effect of auxiliary reinforcement on the face of push-offs.

#### 4.5 Tri-linear model proposal for determining the ultimate shear strength

After evaluating the studies conducted by Mansur et al. [23] in which a tri-linear model was proposed to predict the ultimate shear strength of different types of concrete with varying clamping stress and considering the inclusion of new experimental data, it was developed a new tri-linear approach in Soares [16], using the same limits proposed by Mansur et al. [23].

Each equation proposed by Soares [16] was obtained with the best fit curve, as shown in Figure 13a.

The new tri-linear approach is defined by the equations below.

- for values of  $\rho_v f_{yd}/f_{cm} \leq 0.075$ :

$$\frac{\tau_u}{f_{cm}} = 1.4259 \frac{\rho_v f_{yd}}{f_{cm}} + 0.0377 \tag{1}$$

- for values of  $0.075 \leq \rho_v f_{yd}/f_{cm} \leq 0.27$ :

$$\frac{\tau_u}{f_{cm}} = 0.0154 \frac{\rho_v f_{yd}}{f_{cm}} + 0.2491 \tag{2}$$

- for values of  $\rho_v f_{yd}/f_{cm} > 0.27$ :

$$\frac{\tau_u}{f_{cm}} = 0.24 \tag{3}$$

To compare both models, the following relations were plotted in Figures 13b and 13c  $\tau_{u, \text{exp}}/\tau_{u, \text{cal}}$  for data collected from previous research, including that conducted by Pereira [15] and Soares [16].

A horizontal line has been inserted which intersects the axis in  $\tau_{u, \text{exp}}/\tau_{u, \text{cal}}=1$  which is the optimum value where the calculated and experimental values are equivalent. The points closest to the line refer to the values whose experimental and theoretical data are approximate.

Figures 13b and 13c show the values of the relationship ( $\tau_{u, \text{exp}}/\tau_{u, \text{cal}}$ ) by the tri-linear approach developed by Soares [16] and [23], respectively.

Table 5 shows the statistical parameters of the calculated values of the ( $\tau_{u, \text{exp}}/\tau_{u, \text{cal}}$ ) of the model proposed by Mansur et al. [23], and Soares [16].

**Table 5.** Comparison of statistical parameters obtained according to the equations of Mansur et al. [23] and Soares [16].

Research	Average of $\tau_{u, \text{exp}}/\tau_{u, \text{cal}}$		Standard Deviation		Coefficient of variation (%)	
	[23]	[16]	[23]	[16]	[23]	[16]
[8]	0.92	1.17	0.18	0.22	19.57	18.51
[21]	0.87	0.95	0.43	0.39	49.43	40.86
[23]	0.99	1.06	0.36	0.13	36.36	12.51
[6]	0.79	0.96	0.13	0.14	16.46	14.76
[27]	0.81	0.97	0.18	0.14	22.22	14.16
[22]	0.81	0.97	0.15	0.18	18.52	18.23
[28]	0.77	0.96	0.12	0.15	15.58	15.08
[29]	0.82	1.04	0.13	0.16	15.85	15.46
[15]	0.65	0.77	0.10	0.09	15.38	12.12
[16]	0.63	0.77	0.16	0.22	25.40	28.39
<b>General Average</b>	<b>0.81</b>	<b>0.96</b>				

Analyzing the data from Table 5 and Figure 13b, it can be seen the tri-linear model developed by Soares [16] provides theoretical values closer to the corresponding experimental values.

The overall average obtained for the ( $\tau_{u, \text{exp}}/\tau_{u, \text{cal}}$ ) was 0.81 and 0.96 for Mansur et al. [23] and Soares [16], respectively.

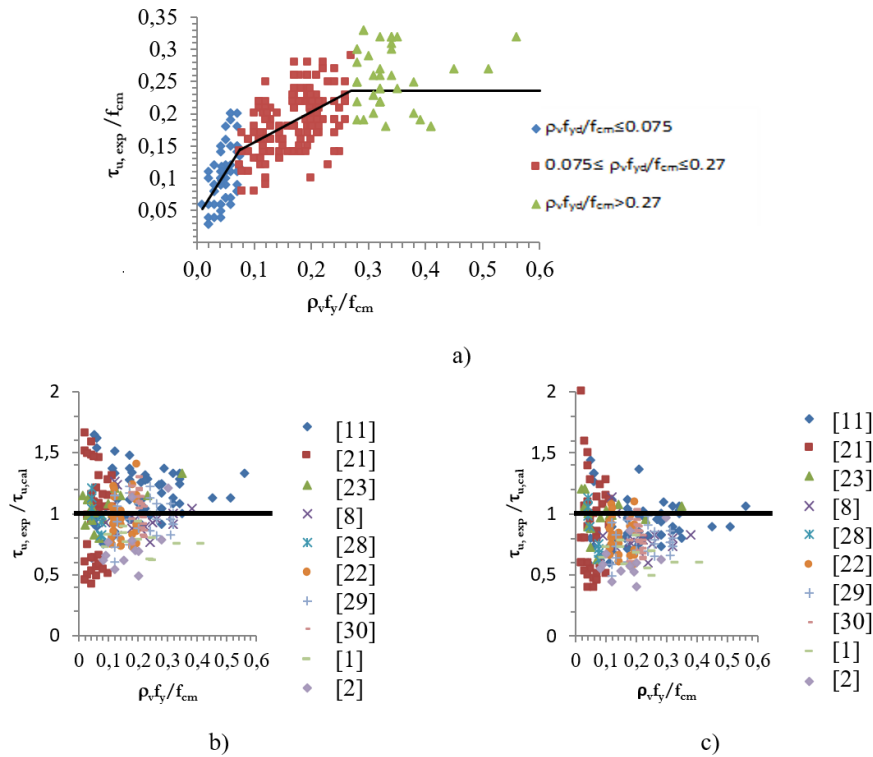


**Figure 13.** Study of tri-linear models to calculate ultimate shear strength: a) model proposed by Soares [16]; b) model results of Soares [16]; c) model results of Mansur et al. [23].

## 5 CONCLUSIONS

This work aimed to analyze shear transfer in sand-lightweight and conventional high-strength concrete. Direct shear tests were performed on push-off specimens for this purpose.

After evaluating the ultimate shear strength results obtained experimentally, comparisons were made with analytical models proposed by previous researchers and the code ACI 318 [14]. It was concluded that:

- the ultimate shear strength increased as the clamping stress increased;
- there was a rise in ultimate shear strength as concrete compression strength increased;
- the code ACI 318 [14] has proven to be conservative, with average values for  $(\tau_{u,exp}/\tau_{u,cal})$  varying from 1.20 (series A) to 1.65 (series B);
- the trilinear model developed by Soares [16] proved to be more effective in the calculation of the ultimate shear capacity, based on the results of the statistical parameters presented, with an overall average of 0.96.

## REFERENCES

- [1] H. W. Birkeland and P. W. Birkeland, "Connections in precast concrete construction," *J. Am. Concr. Inst.*, vol. 63, pp. 345–367, 1966.
- [2] T. T. C. Hsu et al., "Theory of shear transfer strength of reinforced concrete," *ACI Struct. J.*, vol. 84, pp. 149–160, 1987.
- [3] B. González Fonteboa, F. Martínez, D. Carro, and J. Eiras, "Cortante-fricción de los hormigones reciclados Shear friction capacity of recycled concretes," *Mater. Constr.*, vol. 60, no. 299, pp. 53–67, 2010, <http://dx.doi.org/10.3989/mc.2010.49708>.
- [4] P. M. D. Santos and E. N. B. S. Júlio, "A state-of-the-art review on shear-friction," *Eng. Struct.*, vol. 45, pp. 435–448, 2012, <http://dx.doi.org/10.1016/j.engstruct.2012.06.036>.
- [5] J. Wairaven, J. Frenay, and A. Pruijssers, "Influence of concrete strength and load history on the shear friction capacity of concrete members," *PCI J.*, vol. 32, no. 1, pp. 66–84, 1987.
- [6] L. Emiko, V. Thamarakkannan, W. T. Huan, and T. Thangayah, "Shear transfer in lightweight concrete," *Mag. Concr. Res.*, vol. 63, no. 6, pp. 393–400, 2011., <http://dx.doi.org/10.1680/mac.9.00162>.

- [7] A. F. Yang, J.-I. Sim, J.-H. Kang, and A. F. Ashour, "Shear capacity of monolithic concrete joints without transverse reinforcement," *Mag. Concr. Res.*, vol. 64, no. 9, pp. 767–779, 2012., <http://dx.doi.org/10.1680/mac.11.00107>.
- [8] A. H. Mattock, W. K. Li, and T. C. Wang, "Shear transfer in lightweight reinforced concrete," *PCI J.*, vol. 21, no. 1, pp. 20–39, 1976.
- [9] W. C. Tang, T. Y. Lo, and W. K. Chan, "Fracture properties of normal and lightweight high-strength concrete," *Mag. Concr. Res.*, vol. 60, no. 4, pp. 237–244, 2008, <http://dx.doi.org/10.1680/mac.2008.60.4.237>.
- [10] K. H. Yang and K. H. Lee, "Shear friction characteristics and modification factor of concrete prepared using expanded bottom ash and dredged soil granules," *Int. J. Concr. Struct. Mater.*, vol. 13, no. 1, pp. 50, 2019, <http://dx.doi.org/10.1186/s40069-019-0364-x>.
- [11] P. Wu, C. Wu, Z. Liu, and H. Hao, "Investigation of shear performance of UHPC by direct shear tests," *Eng. Struct.*, vol. 183, pp. 780–790, 2019, <http://dx.doi.org/10.1016/j.engstruct.2019.01.055>.
- [12] J. Peng, P. Z. Zhao, S. Wang, S. W. Lee, and S. B. Kang, "Interface shear transfer in reinforced engineered cementitious composites under push-off loads," *Eng. Struct.*, vol. 206, pp. 110013, 2020, <http://dx.doi.org/10.1016/j.engstruct.2019.110013>.
- [13] P. M. D. Santos and E. N. B. S. Júlio, "Interface shear transfer on composite concrete members," *ACI Struct. J.*, vol. 111, no. 1, pp. 113–121, 2014, <http://dx.doi.org/10.14359/51686543>.
- [14] ACI Committee 318, *Building Code Requirements for Structural Concrete*, ACI 318M-14, 2014.
- [15] P. D. S. Pereira, "Avaliação da teoria atrito-cisalhamento em concreto leve e de alta resistência," M.S. thesis, Univ. Est. Norte Fluminense, Campos dos Goytacazes, 2016.
- [16] T. A. Soares, "Teoria atrito-cisalhamento em concretos de diferentes resistências e densidades através do ensaio de *Push-off*," M.S. thesis, Univ. Est. Norte Fluminense, Campos dos Goytacazes, 2018.
- [17] Associação Brasileira de Normas Técnicas, *Análise Granulométrica*, ABNT NBR NM 248, 2003.
- [18] Associação Brasileira de Normas Técnicas, *Agregados – Determinação da Massa Unitária e do Volume de Vazios*, NBR NM 45, 2006.
- [19] Associação Brasileira de Normas Técnicas, *Concreto-Ensaio de Compressão de Corpos-de-prova Cilíndricos*, ABNT NBR 5739, 2007.
- [20] Associação Brasileira de Normas Técnicas, *Argamassa e Concreto – Determinação da Resistência à Tração por Compressão Diametral de Corpos-de-Prova Cilíndricos*, ABNT NBR 7222, 2011.
- [21] L. F. Kahn and A. D. Mitchell, "Shear friction tests with high-strength concrete," *Struct. J.*, vol. 99, no. 1, pp. 98–103, 2002.
- [22] L. H. Shaw and L. H. Sneed, "Interface shear transfer of lightweight-aggregate concretes cast at different times," *PCI J.*, vol. 53, no. 3, pp. 130–144, 2014.
- [23] M. A. Mansur, T. Vinayagam, and K.-H. Tan, "Shear transfer across a crack in reinforced high-strength concrete," *J. Mater. Civ. Eng.*, vol. 20, no. 4, pp. 294–302, 2008, [http://dx.doi.org/10.1061/\(ASCE\)0899-1561\(2008\)20:4\(294\)](http://dx.doi.org/10.1061/(ASCE)0899-1561(2008)20:4(294)).
- [24] A. Gerritse, "Design considerations for reinforced lightweight concrete," *Int. J. Cement Compos. Lightweight Concr.*, vol. 3, no. 1, pp. 57–69, 1981, [http://dx.doi.org/10.1016/0262-5075\(81\)90031-2](http://dx.doi.org/10.1016/0262-5075(81)90031-2).
- [25] C. H. Raths, "Design proposals for reinforced concrete corbels," *PCI J.*, vol. 21, no. 3, pp. 18–42, 1977.
- [26] A. H. Mattock, "Shear friction and high-strength concrete," *ACI Struct. J.*, vol. 98, no. 1, pp. 50–59, 2001, <http://dx.doi.org/10.14359/10146>.
- [27] K. A. Harries, G. Zeno, and B. Shahrooz, "Toward an improved understanding of shear-friction behavior," *ACI Struct. J.*, vol. 109, no. 6, pp. 835–844, 2012, <http://dx.doi.org/10.14359/51684127>.
- [28] S. L. Wermager, "Shear-friction of sand-lightweight clay and slate aggregate concretes with varied reinforcement ratios," M.S. thesis, Missouri Univ. Sci. Technol., Rolla, MO, 2015.
- [29] K. Krc, "An investigation of shear-friction of lightweight aggregate concretes," M.S. thesis, Missouri Univ. Sci. Technol., Rolla, MO, 2015.

---

**Authors contributions:** PSPF, TAS: Fund acquisition, production, data acquisition and analysis; SLGG: conceptualization, supervision and writing; ACSP: writing; JCT: methodology

**Editors:** Leandro Mouta Trautwein, José Luiz Antunes de Oliveira e Sousa, Guilherme Aris Parsekian.